Communication

Segregation-Induced Enhancement of Low-Temperature Tensile Ductility in a Cast High-Nitrogen Austenitic Stainless Steel Exhibiting Deformation-Induced α' Martensite Formation

JAVAD MOLA, MARCO WENDLER, ANDREAS WEIß, BENEDIKT REICHEL, GOTTHARD WOLF, and BRUNO C. DE COOMAN

In spite of the formation of a high fraction of deformation-induced α' martensite, the tensile elongation of a cast high-nitrogen austenitic stainless steel was found to enhance at lower temperatures, a behavior deviating from that exhibited by wrought and homogenized austenitic stainless steels. The observed behavior was explained by the presence of microstructural regions with different stabilities with respect to deformation-induced α' martensite formation caused by the segregation of alloying elements.

DOI: 10.1007/s11661-015-2782-y

Tensile elongation near room temperature of low stacking fault energy (SFE) austenitic steels including stainless,[1–9] high Mn,[10–13] and high Ni[14] steels varies in three temperature regimes as follows. At the highest temperature range (regime I), tensile elongation remains more or less constant or exhibits a weak temperature dependence. At intermediate temperatures (regime II), elongation increases as the temperature decreases. The enhancement of ductility at reduced temperatures in regime II is commonly attributed to such deformation-induced microstructural changes as ε martensite formation, the ε-TRIP effect,[15] and deformation twinning, the TWIP effect.[2] These are common microstructural features of deformed austenitic stainless steels[16,17] and high Mn[12,18,19] steels and are thought to be consequences of high glide planarity. Enhanced glide planarity caused by reduced cross slip of screw dislocations at lower temperatures has been correlated with an underlying temperature dependence of SFE.[20] The latter dependence is available for many fcc metals and alloys including austenitic steels.[20–24] The enhancement of tensile elongation at lower temperatures in regime II of austenitic stainless steels is interrupted at the temperature below which the deformation-induced formation of α' martensite is enabled, namely below the $M_d^{\gamma\to\alpha'}$ temperature. The loss of ductility caused by the deformation-induced formation of α' martensite initiates the regime III of elongation, characterized by reduced elongations at lower temperatures. The large number of investigations in support of the detrimental effect of α' martensite formation on the tensile elongation of metastable austenitic stainless steels[1–7, 10–12] indicates that any possible contribution to the ductility of a TRIP effect would not be large enough to prevent the loss of ductility below the $M_d^{\gamma\to\alpha'}$ temperature. This has been also suggested by the modeling of the α' TRIP effect contribution to the ductility.[25] The present study demonstrates how compositional inhomogeneities in a cast high-nitrogen austenitic stainless steel can cause deviation from the behavior described above.

The chemical composition of the experimental steel was Fe-14.3Cr-5.5Mn-5.5Ni-0.5Si-0.37N-0.02C (mass pct). The high nitrogen content of the steel was achieved by melting under nitrogen pressures up to 4 bar. The high superheating of the molten alloy (2023 K or 1750 °C) and the raised temperature of the mold kept inside the pressurized melting chamber resulted in a slow cooling rate during solidification. Tensile specimens with a gage diameter of 6 mm were subsequently machined from the as-cast ingot with a dimension of $210 \times 80 \times 45$ mm^3. To ensure the absence of deformation-induced martensite at the surface of machined tensile specimens, they were heat treated at 1323 K (1050 °C) for 30 minutes. Using an initial strain rate of 4×10^{-4} s^{-1}, tensile specimens were tensile tested at temperatures between 233 K and 473 K (−40 °C and 200 °C). According to the prior experience of the authors, this strain rate is sufficiently low to ensure negligible adiabatic heating of tensile specimens. Microstructural examination of tensile-tested specimens was performed by means of light optical microscopy, scanning electron microscopy (SEM) including electron backscatter diffraction (EBSD), and transmission electron microscopy (TEM). Quantification of deformation-induced α' martensite in the gage area of tensile-tested specimens was done by magnetic saturation measurements using a Metis MSAT magnetic saturation device equipped with a Lakeshore 480 fluxmeter. Details on the quantification procedure may be found in.[26]

The optical micrograph in Figure 1(a) shows the microstructure prior to tensile experiments. In Figure 1(b), the weakly etched grain boundaries in Figure 1(a) are demarcated by dashed lines. The microstructure consists of dendrites commonly extending across grain boundaries. Thermodynamic calculations using Thermo-Calc with a TCFE7 database (not shown) predicted an austenitic solidification for the alloy. Austenitic mode of solidification was also predicted based on empirical relationships taking into account the ratio of ferrite to austenite

JAVAD MOLA, MARCO WENDLER, Scientific Assistants, and ANDREAS WEIß, Professor, are with the Institute of Iron and Steel Technology, Technische Universität Bergakademie Freiberg, Leipziger St. 34, 09599 Freiberg, Germany. Contact e-mail: javad.mola@iest.tu-freiberg.de BENEDIKT REICHEL, Scientific Assistant, is with the Institute of Materials Science, Technische Universität Bergakademie Freiberg, 09599 Freiberg, Germany. GOTTHARD WOLF, Professor and Director, is with the Foundry Institute, Technische Universität Bergakademie Freiberg. BRUNO C. DE COOMAN, Professor and Director, is with the Materials Design Laboratory, Graduate Institute of Ferrous Technology, Pohang University of Science and Technology, Pohang 790-784, South Korea.

Manuscript submitted November 12, 2014.
Article published online February 10, 2015

stabilizing alloying elements.[27,28] The dendritic morphology in Figures 1((a), (b)) therefore reveals the arrangement of primary dendrites of austenite and interdendritic regions formed at later stages of solidification. The dark spots distributed mainly in interdendritic regions in Figures 1((a), (b)), and shown at a higher magnification in the SEM micrograph of a deformed specimen in Figure 1(c), are primarily undissolved M_2N nitrides (M denoting Cr, Fe, and substitutional alloying elements). Precipitates have coarsened significantly during the slow cooling of the ingot and the subsequent annealing at 1323 K (1050 °C). M_2N precipitates persisted in spite of their being predicted by Thermo-Calc to fully dissolve at 1323 K (1050 °C).

Engineering stress–strain curves for tensile specimens tested at various temperatures are shown in Figure 2(a). At all tensile test temperatures studied, decreasing temperature was associated with simultaneous improvement of strength and ductility. The temperature dependences of the 0.2 pct proof stress ($R_{p0.2}$), tensile strength (R_m), uniform elongation (A_g), and total elongation (A) are shown in Figure 2(b).

In Figure 2(b), the temperature dependence of deformation-induced α' martensite fraction ($f_{\alpha'}$) determined by magnetic saturation measurements is superimposed on tensile properties. Deformation-induced α' martensite only occurred at and below room temperature. The highest deformation-induced α' martensite content of 53 vol pct occurred during tensile deformation at 233 K (−40 °C).

EBSD analysis of selected deformation conditions was performed to study the occurrence of common deformation-induced processes such as twinning and martensite formation. EBSD orientation maps of specimens strained at 373 K and 293 K (100 °C and 20 °C) are shown in Figures 3((a), (b)). No twinning or ε martensite was detected even after EBSD scans using a refined step size of 0.2 μm. Formation of coarse deformation twins in Fe-16Cr-6Mn-(3,6,9)Ni alloys,[29] Fe-19Cr-4Ni-3Mn-0.25C-0.15N alloys,[8,9] and Fe-17Cr-6Mn-0.45C-9Ni-(0,4)Al alloys[30] tensile tested at temperatures above their respective $M_d^{\gamma\rightarrow\alpha'}$ temperatures has been readily confirmed with EBSD scans using step sizes of the order of 0.2 μm. The absence of deformation twins is in agreement with the reported twin-suppressing role of N in Fe-Cr-Ni stainless steels.[31] As shown in Figures 3((c), (d)), 15 pct tensile straining at 233 K (−40 °C) was associated with the formation of both ε and α' martensites. These phases were always observed in the vicinity of one another. In agreement with the magnetic saturation measurement results, tensile straining until fracture at 233 K (−40 °C) was associated with significant α' martensite formation (Figures 3((e), (f)). Figure 3(f) which shows only the orientation map of the austenite phase clearly indicates that transformed regions reproduce the dendritic morphology of Figures 1((a), (b)). The arrows in Figures 3((e), (f)) denote a transformed dendrite core on both sides of an austenite grain boundary. The deformation-induced transformation of dendrite core regions is attributed to the segregation of alloying elements during the formation of primary dendrites of austenite. Segregation of major alloying elements including Cr, Ni, and Mo to the surrounding liquid phase during the formation of primary dendrites of austenite has been observed in an Fe-19Cr-14Ni-2.5Mo cast stainless steel.[32] Manganese has been found to exhibit a similar behavior.[27] Furthermore, the higher concentration of undissolved nitrides in interdendritic regions suggests that the

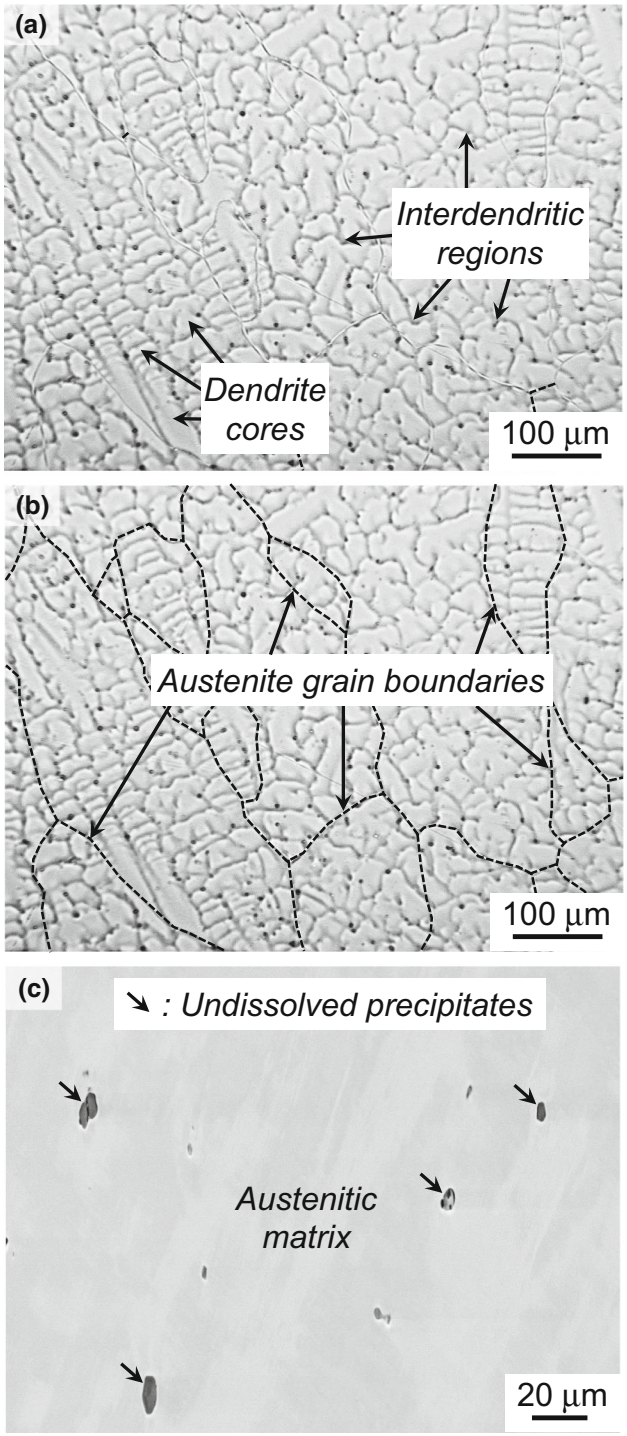

Fig. 1—(*a*, *b*) Light optical and (*c*) scanning electron micrographs of the cast steel. Specimens were electrolytically etched with oxalic acid. The contrast in (c) was generated by secondary electrons.

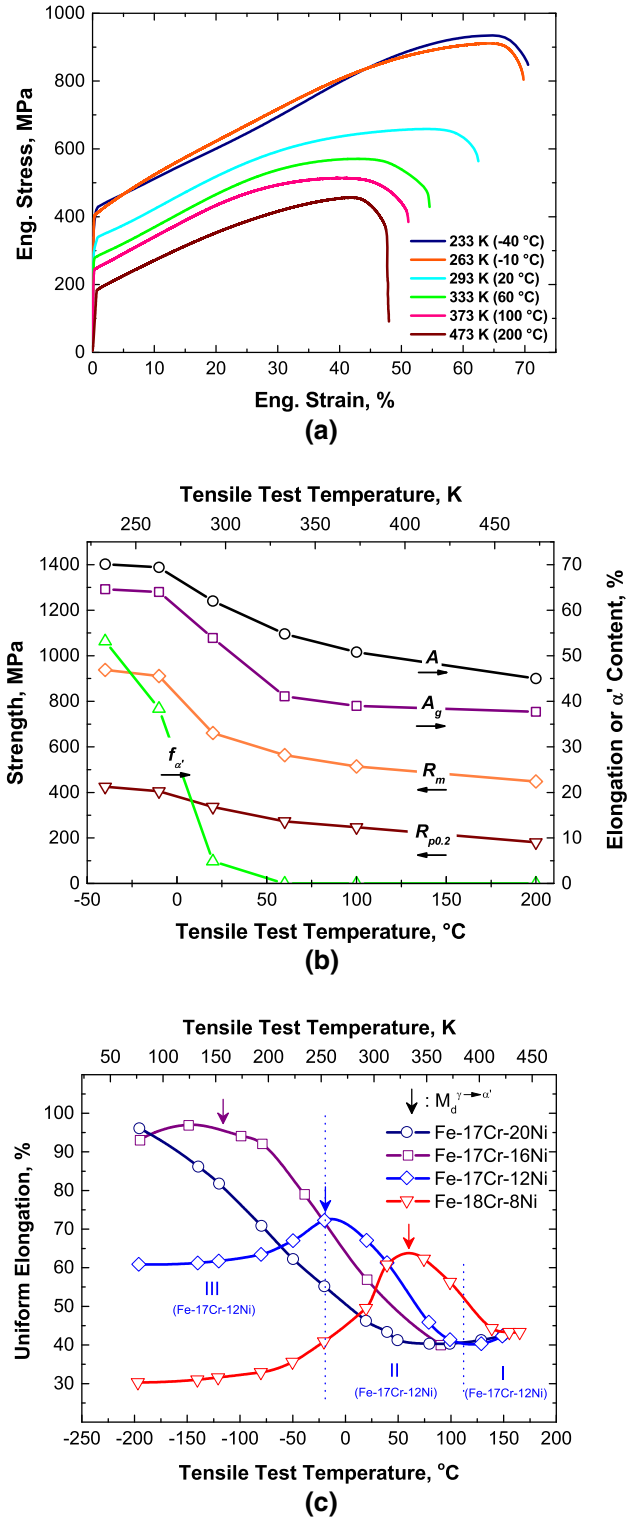

Fig. 2—(*a*) Engineering stress–strain curves for the experimental steel at various temperatures; (*b*) temperature dependence of tensile properties and deformation-induced α′ content; (*c*) temperature dependence of tensile elongation for Fe-(17-18)Cr-Ni alloys with various Ni concentrations adapted from.[33]

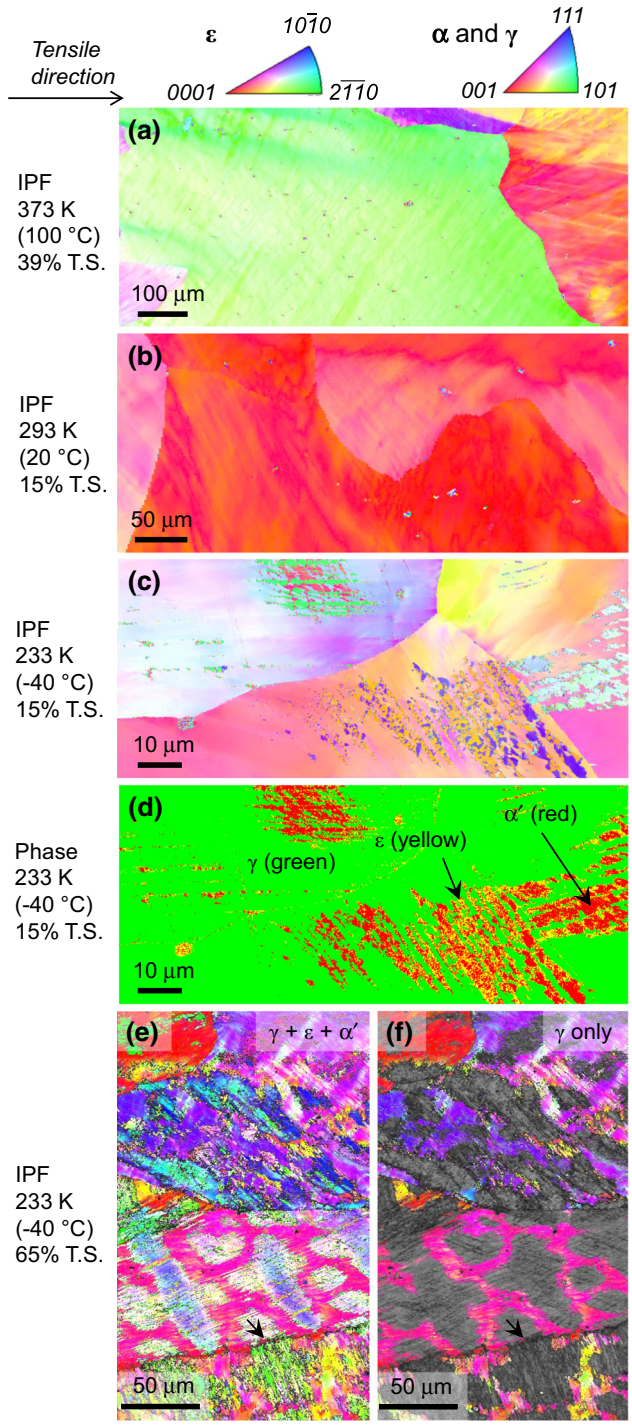

Fig. 3—(*a* through *c*, *e*, *f*) EBSD inverse pole figure (IPF) maps of tensile specimens deformed to indicated tensile strains (T.S.) at temperatures marked. Colors indicate crystal directions parallel to tensile direction; (*d*) phase map corresponding to the IPF in (c).

nitrogen too has segregated out of the growing dendrites of primary austenite. Due to the high diffusivity of nitrogen at the solution annealing temperature of 1323 K (1050 °C) which enables its long range diffusion and homogenization in the austenite, any possible inhomogeneity of N concentration is thought to only arise due to local variations in the solubility of N caused by the segregation of substitutional alloying elements. The distribution of alloying elements had made dendrite core regions favorable sites for the deformation-induced formation of α′ martensite. The alloy can therefore be

regarded as being composed of dendrite core regions with a low stability with respect to the deformation-induced α' martensite formation and farther regions with a higher stability. In other words, the $M_d^{\gamma\rightarrow\alpha'}$ temperature gradually decreases from cores of dendrites toward interdendritic regions.

The localized transformation of dendrite core regions is thought to be responsible for the observation of improved tensile ductility at subzero temperatures where deformation-induced α' martensite formation is enabled (Figure 2(b)). This behavior is inconsistent with the well-documented elongation regimes discussed in the introduction and exemplified with wrought Fe-17Cr-(9-20)Ni stainless steels in Figure 2(c).[33] The marked $M_d^{\gamma\rightarrow\alpha'}$ temperature of Fe-17Cr-(9-20)Ni alloys almost exactly coincides with the temperature of highest tensile elongation. The formation of α' martensite below the $M_d^{\gamma\rightarrow\alpha'}$ temperature thus leads to the onset of ductility regime III characterized by lower elongations at reduced tensile test temperatures.

The temperature dependence of tensile elongation in the present high N alloy is the balance of that at different regions of the microstructure. In fact, the alloy can be visualized as being composed of regions with different temperature dependencies of tensile elongation whose summation according to the rule of mixtures gives the overall temperature dependency of tensile elongation depicted in Figure 2(b). On this basis, the tensile test temperature of 293 K (20 °C) should lie in ductility regime III of the transformed regions (near dendrite cores), whereas it is still in ductility regime II of the more heavily alloyed interdendritic regions. Therefore, although reducing tensile test temperature would have a negative effect on the ductility of dendrite core regions due to the earlier occurrence of deformation-induced α' martensite, it enhances ductility of the more heavily alloyed interdendritic regions by promoting planar glide in the absence of deformation-induced α' martensite formation. The balance of these opposing effects is thought to be responsible for the observed enhancement of ductility in spite of α' martensite formation at 263 K and 233 K (−10 °C and −40 °C).

Two families of steels which are prone to compositional inhomogeneities within austenitic regions are TRIP-assisted and quenched and partitioned (Q&P) steels. Although differences in the stability of austenite in such steels may also arise from differences in such parameters as the size and morphology of retained austenite regions,[34] a scenario analogous to that of the present steel with significant local variations in the stability of retained austenite with respect to martensitic transformation can most likely arise due to local variations in the carbon concentration of retained austenite. Accordingly, in studies involving tensile tests at various temperatures of TRIP-assisted and Q&P steels,[35,36] the observation of highest tensile elongations at temperatures associated with transformation of noticeable fractions of original γ content may be attributed to compositional inhomogeneities within retained austenite rather than a TRIP effect.

The occurrence of ε martensite during low-temperature deformation of the alloy, as suggested by the EBSD

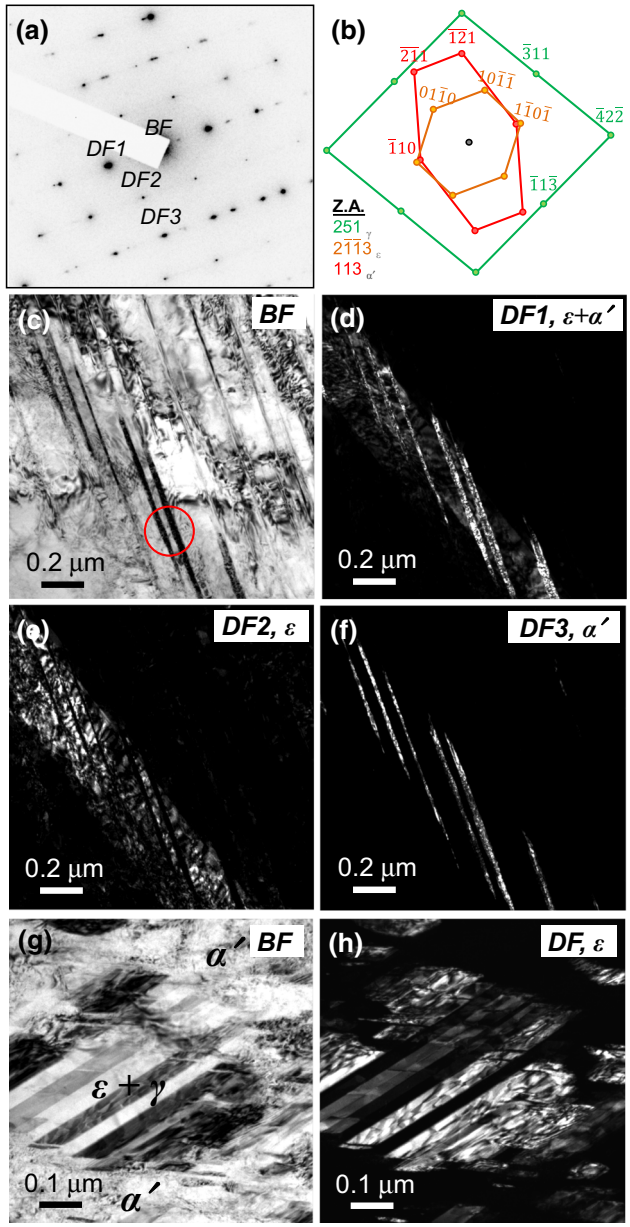

Fig. 4—(*a*) SAD pattern of a specimen tensile strained 15 pct at 233 K (−40 °C). As shown in (*b*), the pattern was found to consist of superimposed reflections of γ, ε, and α' phases. The area used for SAD pattern acquisition is encircled in (*c*). (*d* through *f*) are dark field images recorded using the reflections marked in (a); (*g*) bright field image of a specimen deformed until fracture (65 pct T.S.) at 233 K (−40 °C); (*h*) dark field image of the area shown in (g) recorded using a reflection of ε phase.

phase map of Figure 3(d), was confirmed by complementary TEM examinations. The ε martensite plates appear to be closely connected with the α' martensite formed during tensile tests at and below RT. The selected area diffraction (SAD) pattern in Figure 4(a) whose solution is provided in Figure 4(b) was taken from the encircled region in the bright field image of Figure 4(c) and pertains to a specimen strained 15 pct at 233 K (−40 °C). Shown in Figures 4((d) through (f)) are dark field images corresponding to the bright field image

of Figure 4(c). They were recorded using the reflections marked in Figure 4(a). The wide band illuminated in the dark field image of Figure 4(e) was identified as ε martensite. The thinner plates oriented more vertically with respect to the wide band of ε martensite which are separately shown in the dark field image of Figure 4(f) were found to be α′ martensite. The dark field image in Figure 4(d) was recorded using a common reflection of ε and α′ martensite phases. Although thin plates of α′ martensite can be seen in the bright field image of Figure 4(c) to extend outside the wide ε martensite plate, they do not diffract according to α′ martensite outside the region of intersection. Provided that thinner plates outside the intersection region are another variant of ε martensite, the crystallographic description of deformation-induced $\gamma \rightarrow \alpha'$ transformation *via* intermediate ε martensite[37] may be used to visualize the shears required to accomplish the transformation. TEM examination of a specimen tensile tested until fracture at 233 K (−40 °C) revealed the presence of a high density of ε martensite plates in untransformed austenitic regions. This behavior is exemplified in the bright field image of Figure 4(g). The corresponding dark field image in Figure 4(h) was recorded using a reflection of ε martensite. The dominant occurrence of ε martensite in the deformed microstructure of the investigated high N stainless steel suggests that it acts as precursor to the deformation-induced formation of α′ at larger strains.

In summary, the temperature dependence of tensile elongation in a high-nitrogen cast stainless steel was correlated with microstructural changes during tensile deformation. The observation of enhanced tensile elongation at low temperatures where α′ martensite formation near dendrite core regions was enabled was justified by the presence of interdendritic regions exhibiting superior ductility at reduced tensile test temperatures. The difference in the stability of austenitic regions was caused by elemental segregation during the slow primary solidification of the alloy. Furthermore, the alloy exhibited a high resistance against deformation twinning. In addition to α′ martensite, deformed microstructures at low deformation temperatures contained a high density of ε martensite.

The support of German Research Foundation in the framework of Collaborative Research Center 799 is gratefully acknowledged.

REFERENCES

1. M. Pozuelo, J.E. Wittig, J.A. Jiménez, and G. Frommeyer: *Metall. Mater. Trans. A*, 2009, vol. 40A, pp. 1826–34.
2. A.S. Hamada, L.P. Karjalainen, R.D.K. Misra, and J. Talonen: *Mater. Sci. Eng. A*, 2013, vol. 559, pp. 336–44.
3. A. Jahn, A. Kovalev, A. Weiß, S. Wolf, L. Krüger, and P.R. Scheller: *Steel Res. Int.*, 2011, vol. 82, pp. 39–44.
4. A. Kovalev, A. Jahn, A. Weiß, and P.R. Scheller: *Steel Res. Int.*, 2011, vol. 82, pp. 45–50.
5. A. Kovalev, A. Jahn, A. Weiß, S. Wolf, and P.R. Scheller: *Steel Res. Int.*, 2011, vol. 82, pp. 1101–07.
6. A. Kovalev, A. Jahn, A. Weiß, S. Wolf, and P.R. Scheller: *Steel Res. Int.*, 2012, vol. 83, pp. 576–83.
7. M. Wendler, A. Weiß, L. Krüger, J. Mola, A. Franke, A. Kovalev, and S. Wolf: *Adv. Eng. Mater.*, 2013, vol. 15, pp. 558–65.
8. M. Wendler, J. Mola, B. Reichel, L. Krüger, and A. Weiß: in *HNS 2014*, Hamburg, 2014.
9. M. Wendler, J. Mola, B. Reichel, L. Krüger, and A. Weiß: in *HMnS 2014*, Aachen, 2014, pp. 407–10.
10. A.S. Hamada, L.P. Karjalainen, and M.C. Somani: *Mater. Sci. Eng. A*, 2007, vol. 467, pp. 114–24.
11. S. Curtze and V.-T. Kuokkala: *Acta Mater.*, 2010, vol. 58, pp. 5129–41.
12. O. Grässel, L. Krüger, G. Frommeyer, and L.W. Meyer: *Int. J. Plast.*, 2000, vol. 16, pp. 1391–409.
13. M. Hauser: Diploma Thesis, TU Bergakademie Freiberg, 2013.
14. I. Tamura: *Met. Sci.*, 1982, vol. 16, pp. 245–53.
15. W. Zhang and J. Hu: *Mater. Charact.*, 2013, vol. 79, pp. 37–42.
16. L. Remy and A. Pineau: *Metall. Trans.*, 1974, vol. 5, pp. 963–65.
17. H. Biermann, J. Solarek, and A. Weidner: *Steel Res. Int.*, 2012, vol. 83, pp. 512–20.
18. S. Allain, J.-P. Chateau, O. Bouaziz, S. Migot, and N. Guelton: *Mater. Sci. Eng. A*, 2004, vols. 387–389, pp. 158–62.
19. O. Bouaziz, S. Allain, C.P. Scott, P. Cugy, and D. Barbier: *Curr. Opin. Solid State Mater. Sci.*, 2011, vol. 15, pp. 141–68.
20. F. Abrassart: *Metall. Trans.*, 1973, vol. 4, pp. 2205–16.
21. L. Rémy, A. Pineau, and B. Thomas: *Mater. Sci. Eng.*, 1978, vol. 36, pp. 47–63.
22. R.M. Latanision and A.W. Ruff: *Metall. Trans.*, 1971, vol. 2, pp. 505–09.
23. F. Lecroisey and B. Thomas: *Phys. Status Solidi A*, 1970, vol. 2, pp. K217–20.
24. L. Remy: *Acta Metall.*, 1977, vol. 25, pp. 173–79.
25. H.K.D.H. Bhadeshia: *ISIJ Int.*, 2002, vol. 42, pp. 1059–60.
26. M. Wendler, B. Reichel, R. Eckner, O. Fabrichnaya, L. Krüger, A. Weiß, and J. Mola: *Metall. Mater. Trans. A*, 2014, DOI: 10.1007/s11661-014-2716-0.
27. P.L. Ferrandini, C.T. Rios, A.T. Dutra, M.A. Jaime, P.R. Mei, and R. Caram: *Mater. Sci. Eng. A*, 2006, vols. 435–436, pp. 139–44.
28. J.A. Brooks and A.W. Thompson: *Int. Mater. Rev.*, 1991, vol. 36, pp. 16–44.
29. A. Vinogradov, A. Lazarev, M. Linderov, A. Weidner, and H. Biermann: *Acta Mater.*, 2013, vol. 61, pp. 2434–49.
30. R. Rahimi, B.C. De Cooman, H. Biermann, and J. Mola: *Mater. Sci. Eng. A*, 2014, vol. 618, pp. 46–55.
31. M. Yoshitake, T. Tsuchiyama, and S. Takaki: *Tetsu-to-Hagane*, 2012, vol. 98, pp. 223–28.
32. N. Lewis, M.J. Cieslak, and W.F. Savage: *J. Mater. Sci.*, 1987, vol. 22, pp. 2799–2810.
33. H. Gutte and A. Weiß: *Habilitation*, TU Bergakademie Freiberg, 2011.
34. L. Samek, E. De Moor, J. Penning, and B.C. De Cooman: *Metall. Mater. Trans. A*, 2006, vol. 37A, pp. 109–24.
35. Y. Sakuma, D.K. Matlock, and G. Krauss: *Metall. Trans. A*, 1992, vol. 23A, pp. 1233–41.
36. W. Feng, Z. Wu, L. Wang, and J.G. Speer: *Steel Res. Int.*, 2013, vol. 84, pp. 246–52.
37. T.H. Lee, H.Y. Ha, J.Y. Kang, J. Moon, C.H. Lee, and S.J. Park: *Acta Mater.*, 2013, vol. 61, pp. 7399–7410.